Two-dimensional modeling of long-term transients in inductively coupled plasmas using moderate computational parallelism. II. Ar/Cl_2 pulsed plasmas

Pramod Subramonium[a)]
Department of Chemical Engineering, University of Illinois, 1406 West Green Street, Urbana, Illinois 61801

Mark J. Kushner[b)]
Department of Electrical and Computer Engineering, University of Illinois, 1406 West Green Street, Urbana, Illinois 61801

(Received 30 April 2001; accepted 19 November 2001)

Quantifying transient phenomena such as pulsed operation is important to optimizing plasma materials processing. In particular, pulsed electronegative plasmas are promising candidates for reducing notching and charge buildup in features during microelectronics fabrication. In this article, a two-dimensional plasma equipment model is employed to investigate pulsed inductively coupled plasmas in Ar/Cl_2 gas mixtures. The consequences of varying pulse repetition frequency (PRF), duty cycle, power, pressure, and Cl_2 mole fractions on plasma properties are quantified. The nonmonotonic temporal dynamics in Cl^- density observed in experiments are well captured by the model. We found that for constant peak power, a lower duty cycle resulted in higher peak electron temperatures at the leading edge of the power pulse due to a lower initial electron density at the end of the afterglow. Increasing the PRF produces an increase in the time averaged electron density due to a lower rate of attachment in the afterglow. The inertia of Cl^- ions produces a sluggish response to rapid changes in plasma potential which results in ''islands'' of higher Cl^- density in the periphery of the reactor. The results show that as the Cl_2 fraction increases, the transition from electron–ion to ion–ion plasma is more pronounced. © *2002 American Vacuum Society.* [DOI: 10.1116/1.1434965]

I. INTRODUCTION

Pulsed electronegative plasmas are promising candidates for improving etch processes for microelectronics fabrication.[1–8] Extraction of negative ions from electronegative pulsed plasmas has been proposed as a method to reduce charge buildup in features, thereby reducing undesirable notching and bowing. This is attributed to the fact that negative ions are able to reach deep into features during the power-off phase and neutralize positive charge. The extraction of negative ions during the power-off phase is possible because the electron density and electron temperature drop to sufficiently low values that the plasma potential is too low to confine negative ions. The pulsed discharges of interest are radio frequency (rf) inductively coupled discharges (ICPs) in which the carrier frequency (the power) is pulse-square wave modulated. In Part I [9] we describe a moderately parallel computer model with which we investigated the characteristics of pulsed electropositive plasmas in argon. Previous works on the pulsed plasmas of interest are reviewed Part I. Additional works of interest to pulsed electronegative are noted below. [In the discussion that follows, the pulse repetition frequency (PRF) refers to the number of power-on, power-off modulation periods per second. The duty cycle refers to the fraction of the modulation period the power is on. The peak power refers to the maximum instantaneous power applied during the power-on portion of the pulse.]

Overzet *et al.*[1] performed time resolved measurements of pulsed ICPs sustained in SF_6 at 30 mTorr with a power deposition of 150 W at a PRF of 100 Hz, duty cycle of 50%, and flow rate of 20 sccm. They observed a large negative ion flux to the walls immediately at plasma turnoff, which they attributed to a momentary reversal of the sheath electric fields. Samukawa *et al.*[2–4] observed highly selective, anisotropic, notch-, and damage-free polycrystalline silicon etching using chlorine at a pressure of 2 mTorr in a pulsed electron cyclotron resonance (ECR) plasma. Measurements were performed for peak powers of 1 kW at 2.45 GHz, duty cycle of 50%, and PRFs between 10 and 100 kHz.

Takahashi *et al.*[5] investigated pulse modulated ECR plasmas for SiO_2 etching using CHF_3 at 2 mTorr for a peak power of 1 kW at 2.45 GHz, duty cycle of 50%, and PRFs between 10 and 100 kHz. They obtained high selectivity of SiO_2 over Si etching while reducing the effects of microloading. The ratio of CF_2/F they measured largely depended on the duty cycle. Mieno and Samukawa [6] studied pulsed ECR plasmas in Ar/Cl_2 mixtures at 2 mTorr for a peak power of 1 kW at 2.45 GHz, while varying duty cycles and PRFs between 2.5 and 100 kHz. They confirmed that in pulsed Cl_2 plasmas, fluxes of negative ions to the substrate can be obtained as the plasma potential decays in the off period.

Malyshev *et al.*[7] investigated the temporal dynamics of pulsed Cl_2 ICPs at pressures of 3–20 mTorr with an average

a)Electronic mail: subramon@uiuc.edu
b)Author to whom correspondence should be addressed; electronic mail: mjk@uiuc.edu

power of 300 W, PRF of 10 kHz, and duty cycle of 50%. They observed a large degree of modulation in the electron density during the on–off period as a result of the combined effects of loss of electrons by ambipolar diffusion and dissociative attachment. Malyshev and Donnelly [8] also reported on the dynamics of pulsed Cl_2 ICPs operated with a continuous rf substrate bias. The conditions were 10 mTorr, average power of 500 W at 13.56 MHz, duty cycle of 50%, and PRFs between 0.3 and 10 kHz. The rf bias power was 300 W. They found that there is no significant difference in plasma characteristics with or without the rf bias during the on period. In the off period with a rf bias, the electron temperature increased rapidly in the late afterglow after having dropped in the early after glow. The electron and ion densities decreased in the early off period with or without the bias. The electron density decreased more rapidly in the late afterglow with a rf bias.

These previous results show that pulsed electronegative plasmas have unique features that can be tailored by judicious choice of gas composition, PRF, duty cycle, and power. In this article, results from our computational investigation of Ar/Cl_2 pulsed ICPs are presented to demonstrate some of these properties. This study was performed with the two-dimensional hybrid model employing moderate computational parallelism described in Part I. Transients in electropositive plasmas are discussed in Part I. Here, we extend that study to electronegative plasmas. Our computational method directly interfaces short plasma time scales (sub-ns) with long-term neutral time scales (ms). The short time scales are determined by resolving the plasma frequency and oscillations in the rf potential. The long time scales are determined by transport of neutral species across the reactor. Briefly, in this numerical method plasma transport, neutral fluid transport, and electromagnetics are simultaneously addressed on separate processors of a parallel computer. Fluid properties (e.g., changes in pressure, mole fractions, and flow fields) which slowly evolve over time are made available to the simultaneous calculation of more rapidly changing plasma properties (e.g., electron and ion density, electrostatic fields) through shared memory. This approach thereby captures the long-term transients that occur during pulsed operation of plasmas while still resolving plasma phenomena during a rf cycle.

The results discussed here were performed for a Gaseous Electronics Conference Reference Cell (GECRC) modified to include an inductive coil.[10] The effect of varying duty cycle, PRF, power, pressure, and Cl_2 fraction on plasma properties was quantified. We found that the transition from electron–ion plasma to ion–ion plasma can be controlled by varying PRF. For example, the plasma becomes more electronegative during the power-off period at lower PRF. The electron density peaks off axis during the power-on phase and the peak gradually shifts toward the center of the reactor in the late afterglow. We also observed that the transition from an electron–ion to an ion–ion plasma was shortened as the Cl_2 fraction increased. At Cl_2 fraction at and above 70%, the negative ion flux to the substrate becomes nearly equal to the positive ion flux during the power-off period.

A brief description of the model is presented in Sec. II. The two-dimensional dynamics of pulsed Ar/Cl_2 plasmas are discussed in Sec. III. Our concluding remarks are in Sec. IV.

II. DESCRIPTION OF MODEL

A moderately parallel implementation of the Hybrid Plasma Equipment Model (HPEM)[11–13] was used in this investigation. The parallel HPEM model (HPEM-P) is described in detail in Part I. The structure of the model will be briefly described here. ''Task parallelism'' is employed in HPEM-P to execute the Electromagnetics Module (EMM), Electron Energy Transport Module (EETM), and Fluid Kinetics Module (FKM) of the HPEM in parallel as different tasks on three processors of a symmetric multiprocessor computer having shared memory. The model is implemented using the compiler directives provided in OPENMP[14] for shared memory parallel programming. In doing so, parameters from the different modules can be exchanged through shared memory on a frequent and, in some cases, arbitrarily specified basis without interrupting the time evolving calculation being performed in any other module. For example, the plasma conductivity and collision frequency are continuously updated during execution of the FKM. These updated parameters are made available in shared memory as they are computed so that they can be accessed by the EMM to produce nearly continuous updates of the electromagnetic fields. These more frequent updates of the electromagnetic fields are then made available to the Monte Carlo simulation of the EETM, through shared memory, along with parameters from the FKM to continuously update electron impact source functions and transport coefficients. The electron impact source functions and transport coefficients computed in the EETM are then transferred to the FKM through shared memory, as they are updated, to compute densities, fluxes, and electrostatic fields. Using this methodology, the parameters required by different modules are made available ''on the fly'' from other modules. The methodology adequately captures long-term transients as it directly interfaces the short scale plasma time scales with the long-term neutral time scales.

III. Ar/Cl_2 PULSED PLASMAS

Results from our parametric study of Ar/Cl_2 pulsed plasmas are discussed in this section. The base case conditions are $Ar/Cl_2 = 80/20$ at 20 mTorr, peak power of 300 W, PRF of 10 kHz, and duty cycle of 50%. The reactor is the GECRC discussed in Ref. 10. The Ar/Cl_2 reaction chemistry is given in Table I. Dissociative attachment of Cl_2,

$$e + Cl_2 \rightarrow Cl + Cl^- \quad (1)$$

has a rate coefficient which increases with decreasing electron temperature. This rate of dissociative attachment determines the temporal evolution of electron density and ion density in the afterglow. In the discussion which follows, quasisteady state refers to having achieved a constant density

TABLE I. Ar/Cl_2 chemistry.[a]

Reaction	Rate coefficient ($cm^{-3}\,s^{-1}$)	Reference
$e+Ar\rightarrow Ar^*+e$	b	16
$e+Ar\rightarrow Ar^++e+e$	b	17
$e+Ar^*\rightarrow Ar^++e+e$	b	18
$e+Ar^*\rightarrow Ar+e$	b	d
$Ar^*+Ar^*\rightarrow Ar^++Ar+e$	5×10^{-10}	c
$Ar^++Ar\rightarrow Ar+Ar^+$	5.7×10^{-10}	e
$e+Cl_2\rightarrow Cl^-+Cl$	b	19
$e+Cl_2\rightarrow Cl+Cl+e$	b	19
$e+Cl_2\rightarrow Cl_2^++e+e$	b	19
$e+Cl\rightarrow Cl^*+e$	b	19
$e+Cl\rightarrow Cl^++e+e$	b	19
$e+Cl^*\rightarrow Cl^++e+e$	b	19
$Cl^*\rightarrow Cl$	$1.0\times10^{5}\,s^{-1}$	c
$e+Cl^-\rightarrow Cl+e+e$	b	19
$e+Cl_2^+\rightarrow Cl+Cl$	$1.0\times10^{-7}/T_e^{1/2}$	c
$Cl^-+Cl^+\rightarrow Cl+Cl$	1.0×10^{-7}	c
$Cl^-+Cl_2^+\rightarrow Cl_2+Cl$	1.0×10^{-7}	c
$Cl_2+Ar^*\rightarrow Cl_2^++Ar+e$	7.1×10^{-10}	c
$Cl^-+Ar^+\rightarrow Cl+Ar$	1.0×10^{-7}	c
$Cl+Ar^*\rightarrow Cl^*+Ar$	7.0×10^{-10}	c
$Cl_2+Ar^+\rightarrow Cl_2^++Ar$	8.4×10^{-9}	20
$Cl_2+Ar^+\rightarrow Cl^++Cl+Ar$	6.4×10^{-9}	20
$Cl+Ar^+\rightarrow Cl^++Ar$	2.0×10^{-10}	20
$Cl+Cl+Ar\rightarrow Cl_2+Ar$	$1.28\times10^{-32}\,cm^6/s$	20
$Cl+Cl+Cl\rightarrow Cl_2+Cl$	$1.28\times10^{-32}\,cm^6/s$	21
$Cl+Cl+Cl_2\rightarrow Cl_2+Cl_2$	$5.4\times10^{-32}\,cm^6/s$	21
$Cl^++Cl_2\rightarrow Cl_2^++Cl$	5.4×10^{-10}	c, 20
$Cl^++Cl\rightarrow Cl+Cl^+$	1.0×10^{-9}	c
$Cl_2^++Cl_2\rightarrow Cl_2+Cl_2^+$	0.8×10^{-9}	c

[a]Only reactions that change the density of a species are shown. All pertinent electron impact processes, such as elastic collisions and vibrational excitation, are included in the EMCS.
[b]Rate coefficients are calculated from electron energy distribution obtained in the EMCS. T_e is the electron temperature (eV).
[c]Estimated.
[d]Cross section obtained by detailed balance.
[e]Rate coefficient obtained from mobility. See Ref. 22.

averaged over a rf cycle. Pulse-periodic steady state refers to replicating intrapulse time dependent behavior during successive pulses.

The electron density for the base case conditions at the reference point of the reactor located 1.7 cm radius and 2.3 cm above the substrate [see Fig. 3(a) of Part I] is shown in Fig. 1(a) for duty cycles of 10%, 30%, 50%, and 70%. Unlike the pure argon case discussed in Part I where the quasisteady state during a pulse was reached at a duty cycle of 30%, here the power-on time is not sufficient to reach the quasisteady state for duty cycles of less than 70%. These trends agree well with the experimental results of Hebner and Fledderman.[15] The longer time to achieve a steady state, as well as a pulsed-periodic steady state, is due to the lower ionization rate for a given power deposition of this Ar/Cl_2 gas mixture compared to that for pure argon. In spite of the ionization potential of Ar being 16 eV, the effective ionization potential at the beginning of the power-on pulse in pure Ar is 4–5 eV due to the multistep ionization resulting from a large density of $Ar(4s)$ surviving to the end of the afterglow.

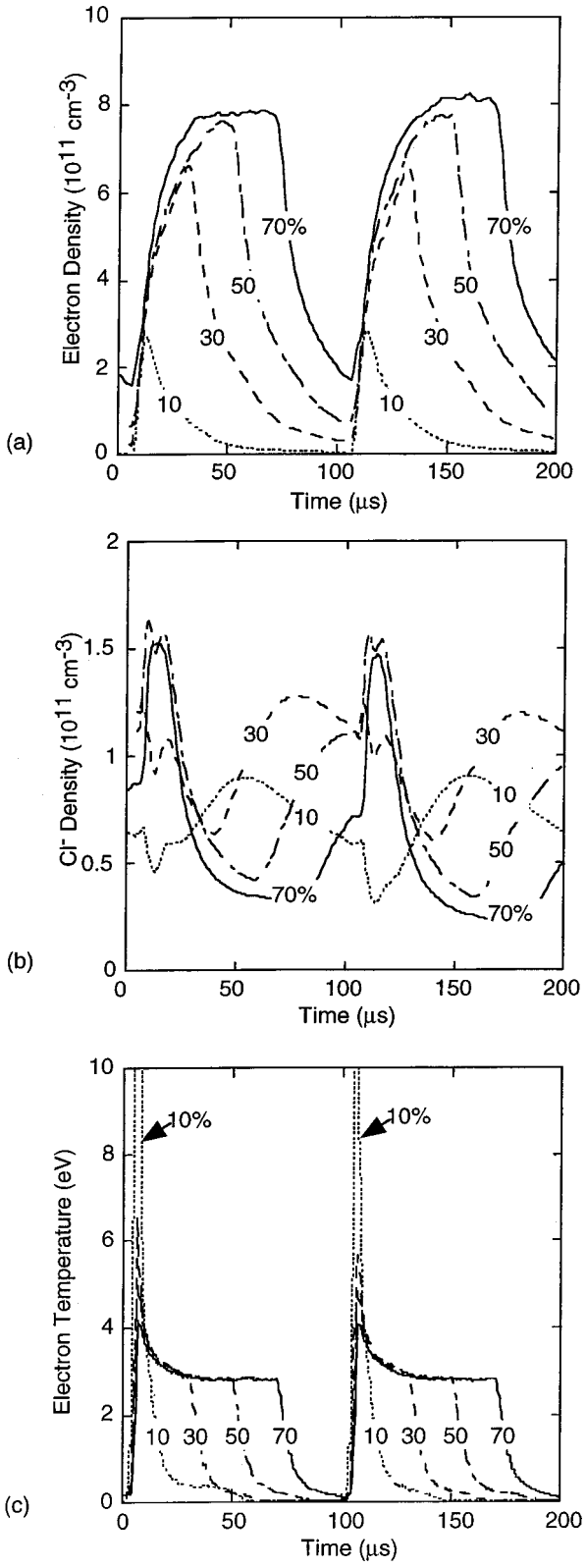

FIG. 1. Plasma properties in an Ar/Cl_2 ICP as a function of time for different duty cycles for a constant peak power of 300 W, PRF of 10 kHz, and gas flow of 20 sccm: (a) electron density at the reference point [Fig. 3(a) Ref. 9], (b) Cl^- density at the reference point, and (c) electron temperature. Quasisteady state electron densities are obtained for duty cycles $\geqslant$50%. The electron temperature peaks more prominently at lower duty cycle due to the lower electron density at the end of the afterglow.

Therefore a large rate of ionization is obtained with a moderate electron temperature. In this Ar/Cl_2 mixture, the effective ionization potential is actually higher than that of pure Ar, in spite of the lower ionization potential of Cl and Cl_2, due to the quenching of $Ar(4s)$. When coupled with dissociative attachment to Cl_2 and power losses due to vibrational and electronic excitation of Cl_2, a lower rate of avalanche occurs. Note that as the duty cycle increases the time averaged power deposition increases, resulting in more dissociation of Cl_2 and less dissociative attachment. A higher electron density is then achieved for a given peak power.

For a given duty cycle and PRF, electron attachment to Cl_2 in the afterglow results in a lower electron density relative to the pure Ar plasma. This lower electron density produces a more highly peaked electron temperature at the leading edge of the following power-on pulse, as shown in Fig. 1(c), as the ICP power is coupled into a smaller inventory of electrons.

The temporal dynamics of the Cl^- density at the reference point are shown in Fig. 1(b). The time dependent Cl^- density significantly varies with different duty cycles. The Cl^- density generally peaks as the power is turned on. This is a bit of an artifact of observing the density in the middle of the plasma because the total inventory of Cl^- does not commensurately change. The plasma potential increases at the beginning of the power-on period, resulting in the negative ions drifting to the center of the plasma where the plasma potential is most positive. Since the plasma potential is absolutely most positive at the start of the power on period, a peak in the Cl^- density results. As the electron temperature decreases following its peak at the start of the power-on period, the peak in plasma potential falls and spatially broadens, resulting in a broader spatial distribution of Cl^- and a decrease in its density at the reference point. A lower rate of dissociative attachment due to the high electron temperature and larger rate of detachment of Cl^- may produce a net decrease of Cl^- density late during the power-on pulse. When the power is turned off, the Cl^- density rises as the rate of dissociative attachment increases with a decrease in the electron temperature. At lower duty cycles, the off time is sufficiently long for the ambipolar diffusion losses of Cl^- to overcome the production of Cl^- ions by dissociative attachment, while the production of Cl^- diminishes due to the depletion of electrons. As a result the Cl^- density may decrease in the late afterglow. These nonmonotonic dynamics agree well with the trends observed by Malyshev *et al.*[7]

The plasma potential and electron temperature display similar transient behavior. When the power is turned off, the plasma potential and electron temperature decay rapidly. The decay in electron temperature is due to loss of electron energy resulting from inelastic collisions and some amount of diffusion cooling [see Fig. 1(c)]. The rate of decay of electron temperature is nearly the same for all duty cycles as the rate depends primarily on the collision frequency which scales with pressure. The decay time of the electron temperature was about 30 μs while the rise time was about 4 μs and was similar for different duty cycles. For 10% duty cycle, the

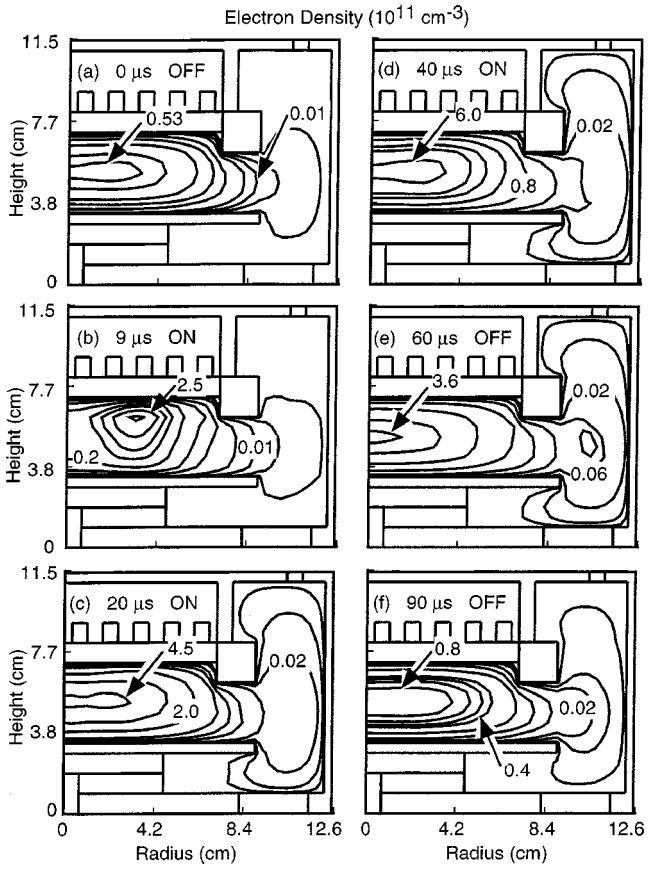

FIG. 2. Electron density in Ar/Cl_2 plasmas at different times for 300 W, PRF of 10 kHz, and duty cycle of 50%. The power is turned off at 50 μs. Results are shown for: (a) 0 μs, (b) 9 μs, (c) 20 μs, and (d) 40 μs during the power-on period and (e) 60 μs and (f) 90 μs during the afterglow. Contours are labeled in units of 10^{11} cm^{-3}.

electron temperature and plasma potential peak exceptionally high at power turn on. The heating rate for a 10% duty cycle is about 10 MeV s^{-1}, resulting from the instantaneous power deposition in the smaller inventory of electrons surviving to the end of the longer afterglow. For example, the electron density for the 10% duty cycle decays to 3×10^9 cm^{-3} at the end of the afterglow, which is 2 orders of magnitude lower than for 70% duty cycle.

The two-dimensional spatiotemporal dynamics of electron and Cl^- densities for the base case conditions are shown in Figs. 2 and 3, respectively. Similar to the pure Ar case discussed in Part I, as the power is turned on, the electron density increases and the peak in electron density occurs under the coil as the majority of power deposition occurs there. The peak is more pronounced compared to the pure Ar case due to the shorter energy relaxation distance of electrons and the continued losses to attachment. [In Ar, the dissipation of electron energy is dominated by collisions with $Ar(4s)$. In Ar/Cl_2 mixtures, this dissipation is dominated by collisions with Cl_2, a process having a shorter mean free path.] As time progresses in the active glow, a quasisteady state is attained with the plasma having an electronegative core and electropositive periphery. At this time the peak in electron density is about 6.0×10^{11} cm^{-3} and is at the center of the reactor.

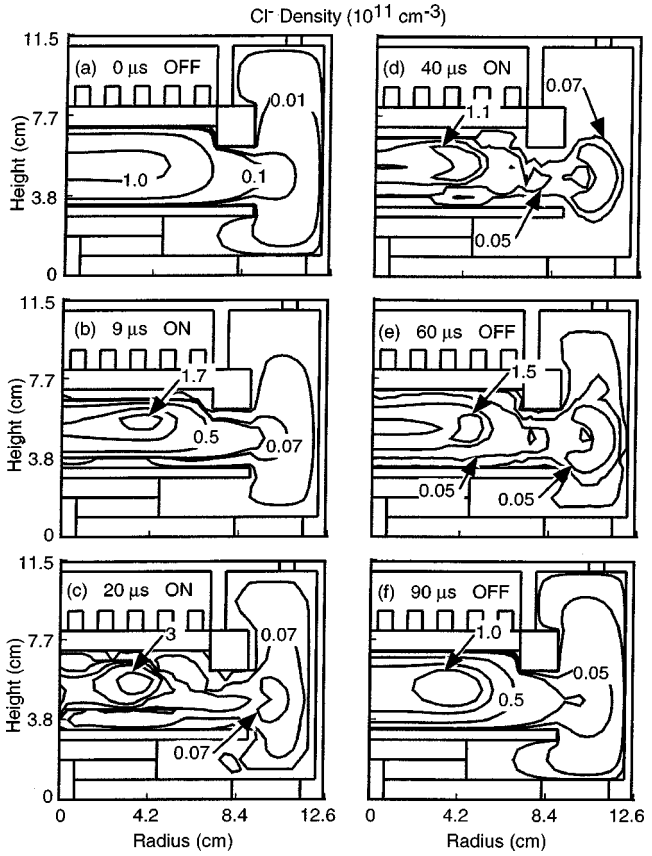

FIG. 3. Cl^- density in Ar/Cl_2 plasmas at different times for 300 W, PRF of 10 kHz, and duty cycle of 50%. The power is turned off at 50 μs. Results are shown for: (a) 0 μs, (b) 9 μs, (c) 20 μs, and (d) 40 μs during the power-on period and (e) 60 μs and (f) 90 μs during the afterglow. Contours are labeled in units of 10^{11} cm^{-3}. Note the ''islands'' of Cl^- ions in the periphery of the reactor due to the inertia of the heavy ions.

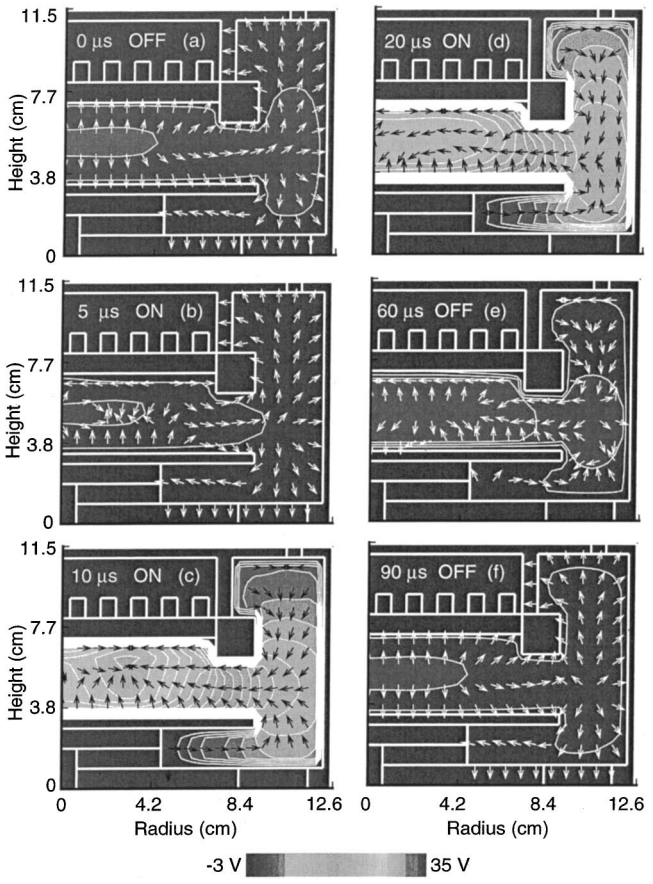

FIG. 4. Cl^- flux vectors and plasma potential in Ar/Cl_2 plasmas at different times for a power of 300 W, PRF of 10 kHz, and duty cycle of 50%. (Cl^- flux vectors only indicate direction and are not scaled with respect to magnitude). Results are shown for: (a) 0 μs, (b) 5 μs, (c) 10 μs, and (d) 20 μs during the power-on period and (e) 60 μs and (f) 90 μs during the afterglow. Negative ions are extracted only after 70 μs into the afterglow.

At power on, the negative ions are accelerated toward the peak of the plasma potential. This produces a local maximum in Cl^- under the coils at 20 μs. However, due to the inertia of the ions, there is still a significant number of ions in the outer regions of the reactor which do not move to the center of the plasma. The acceleration of the ions scales with the electric field which is at best a few V/cm in periphery. In these fields, it would take about 25 μs for the negative ions to move to the center of the plasma from the periphery. However, the electric fields in the periphery fall to a few tenths V/cm in less than this time. Hence, the negative ions are left behind, producing an ''island'' of negative ions in the periphery of the reactor.

As the power is turned off, electrons are rapidly lost due to ambipolar diffusion and dissociative attachment while the negative ion density increases. The plasma transitions from an electron–ion plasma to an ion–ion plasma late in the afterglow. [Compare Figs. 2(f) and 3(f)]. The peak Cl^- density in the late afterglow is 1×10^{11} cm^{-3}, while the electron density is 8×10^{10} cm^{-3}. Prior to power on at the end of the afterglow, the Cl^- density has a diffusion dominated spatial distribution. As a result of the low plasma potential, Cl^- extends throughout the reactor.

The spatiotemporal dynamics of the Cl^- at different times during the pulse are illustrated in Fig. 4 with the flux vectors shown superimposed on the plasma potential. (The vector symbols only indicate the direction of the flux, not its magnitude.) At the end of the afterglow the plasma potential is sufficiently small that low temperature Cl^- ions are able to flow to all the surfaces and the flux vectors point outward. When the power is turned on, the plasma potential increases most rapidly in the center of the plasma where the electron temperature is the highest. The negative ion flux vectors reverse in the center of the reactor where the resulting ambipolar fields are the largest. The ions are accelerated toward the peak in plasma potential under the coils quickly turning away from surfaces as shown in Fig. 4(b). At this early time, negative ions in the periphery are also accelerated toward the center of the plasma. However the electric fields in the periphery are weak (0.6 V/cm) and inertia prevents the heavy ions from immediately following the changes in the plasma potential. For example, negative ions are still moving toward the wall 5 μs in the periphery of the reactor while Cl^- ions in the center of the reactor are moving toward the peak in the plasma potential. At about 10 μs after the power on, the negative ions are moving away from surfaces and toward the

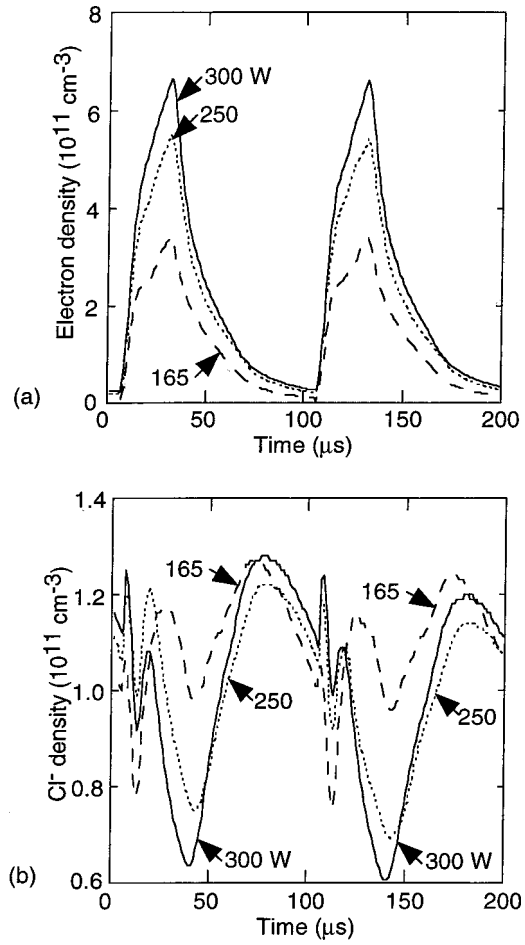

FIG. 5. Plasma properties in Ar/Cl_2 as a function of time for different peak powers for a PRF of 10 kHz, duty cycle of 30%, and gas flow of 20 sccm: (a) electron and (b) Cl^- density at the reference point.

peak in plasma potential under the coil at all reactor locations. The peak in plasma potential moves to the axis as the quasisteady state is achieved (>20 μs). The ion flux vectors track the motion of the peak in plasma potential and, after an inertial lag, also point toward the center.

When the power is turned off at 50 μs, Cl^- ions in the center of the plasma begin moving toward the walls as the electron temperature and plasma potential decrease, and negative ions begin to dominate the negative charge. Cl^- ions in the periphery still move toward the center of the plasma after the power is turned off because of their inertia in the lower electric fields. After 90 μs, the plasma potential has been significantly reduced throughout the reactor for a long enough period of time that the negative ion flux is directed toward surfaces at all locations.

The effect of peak power on plasma properties was investigated from 165 to 300 W. The conditions were 20 mTorr, PRF of 10 kHz, and duty cycle of 30%. The maximum electron density during the power-on pulse scales nearly linearly with power as shown in Fig. 5(a). The power-on time is not long enough to establish a quasisteady state in all cases. The Cl^- density as a function of time for different powers is shown in Fig. 5(b). The Cl^- density is lower in the late active glow at higher power as the Cl_2 undergoes more dissociation and so there is less Cl_2 available to form Cl^- through dissociative attachment. The time at which the Cl^- density peaks in the afterglow was nearly the same for all the cases. The time of this peak corresponds to establishing a balance between losses due to ambipolar diffusion and generation due to dissociative attachment. These two processes are dependent on the electron temperature in the afterglow, which was nearly the same for all powers.

The electronegativity of the plasma increases as the plasma transitions from an electron–ion plasma in the power-on period to an ion–ion plasma in the late afterglow of the power-off period. The electronegativity in the late afterglow is higher at lower power as there is more Cl_2 available for attachment. For example, at 70 μs into the afterglow, the ratio of the Cl^- density to the electron density at the reference point was 3.7 for a power of 300 W, while it was 7.8 for a power of 165 W. The plasma potential peaked at around 40 V and the electron temperature at about 7 eV during the leading edge of the power-on pulse for all powers. The plasma potential and electron temperature peak under the coils where the power deposition is largest. The spatial distributions of electron temperature and plasma potential were similar for all three powers.

The effect of PRF was investigated from 5 to 20 kHz for a peak power of 300 W and 50% duty cycle. The time evolution of electron and Cl^- densities at the reference point are shown in Fig. 6 for PRFs of 5, 10, and 20 kHz. As the PRF was lowered to 5 kHz from the base case value of 10 kHz, a quasisteady state was achieved during the active glow. As the PRF was increased to 20 kHz, a quasisteady state was not achieved. The electron decay rate is similar for all PRFs as the Cl_2 density and rate of attachment are similar. However, as the power is off for a longer time for 5 kHz, the electron density decays to lower values. The peak in Cl^- density in the initial phase of the power turn-on period was about the same for 10 and 20 kHz. The Cl^- density in the late afterglow is also similar for the higher PRFs. However, at 5 kHz, the power-off time is long enough that the plasma potential decays to sufficiently small values that diffusion losses dominate over the production of negative ions by dissociative attachment. As a result, the negative ion density reaches a peak at about 50 μs after plasma turn off while sources due to dissociative attachment are still large, and then decreases due to diffusion losses. Similar processes occur at the higher PRFs, however the final outcome is truncated due to the shorter power-off period. At 10 kHz the Cl^- density has just reached its maximum at the end of the afterglow. For 20 kHz, the Cl^- density is still rising at the end of the afterglow as negative ion generation due to dissociative attachment still dominates over diffusion. As a consequence, a maximum in negative ion density in the afterglow is not observed.

The spatial distribution of electron and Cl^- densities in the late afterglow are shown in Fig. 7 for different PRFs. The transformation from an electron–ion plasma during the power-on period to an ion–ion plasma in the power-off period was more definitive at lower PRFs, as indicated by

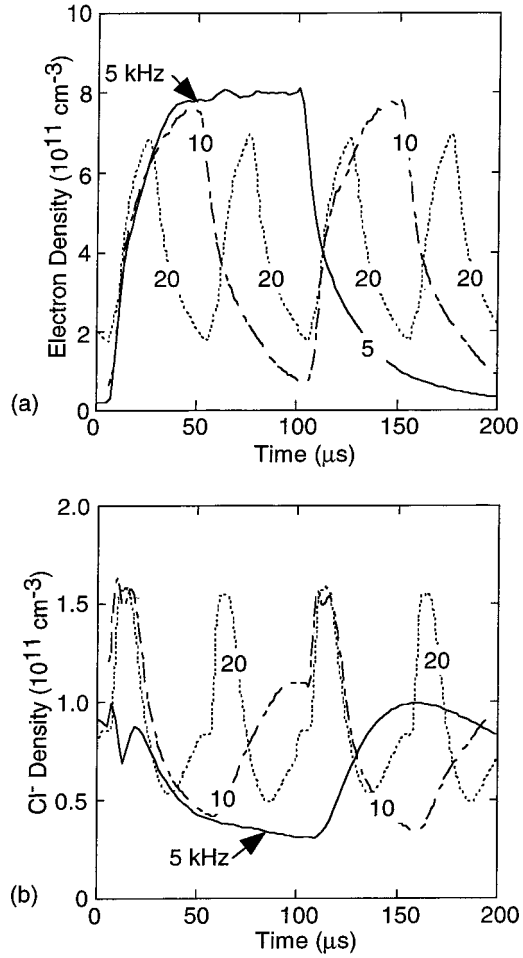

FIG. 6. Plasma properties in Ar/Cl_2 as a function of time for different PRFs for a peak power of 300 W, duty cycle 50%, and gas flow 20 sccm: (a) electron and (b) Cl^- density at the reference point.

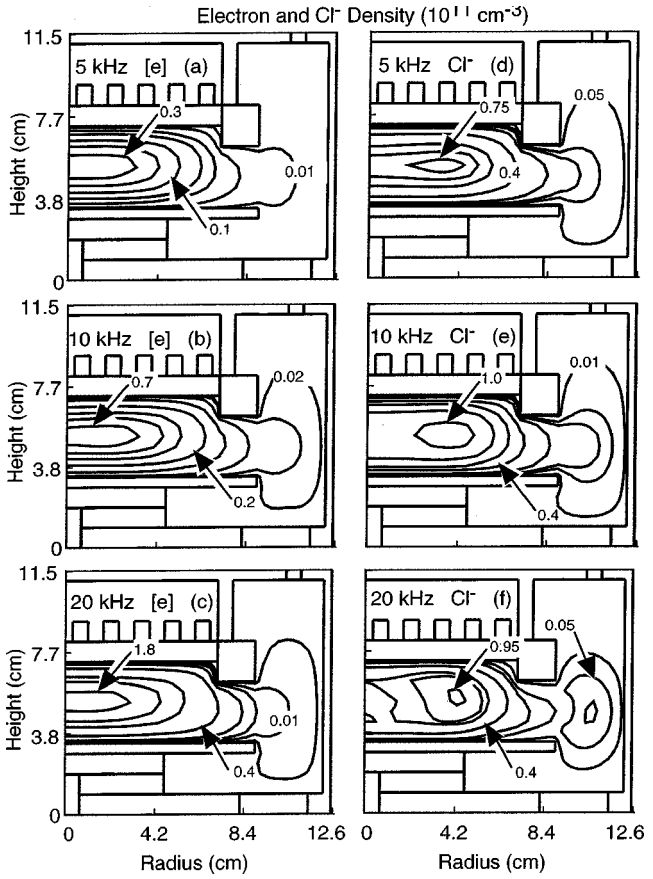

FIG. 7. Electron density (a)–(c) and Cl^- density (d)–(f) in Ar/Cl_2 plasmas in the late afterglow as a function of PRF for a peak input power of 300 W and duty cycle of 50%. Results shown are at the end of afterglow for (d) 5 kHz, (e) 10 kHz, and (f) 20 kHz.

$[Cl^-]>[e]$. The longer power-off periods at the lower PRFs afford more opportunity for the electron density to decay by attachment and for the plasma to become electronegative. In contrast, at 20 kHz, the plasma is still largely electropositive ($[Cl^-]<[e]$) in the late afterglow. Note that at 20 kHz the Cl^- still has an island of higher density in the periphery of the reactor at the end of the afterglow, a structure which has dissipated at the lower PRFs. These structures are due to the inertia of the ions limiting their ability to move to the center of the plasma during the power-on period. These lobes are particularly prevalent at higher PRFs as the negative ions have less time to respond to the changes in the plasma potential.

The peak in the electron temperature is higher at lower pulse repetition frequencies as the power deposition is into a smaller total number of electrons which survive to the late afterglow. The rates of decay of plasma potential and electron temperature are similar for all PRFs as the rate depends primarily on the electron collision frequency which is not a function of PRF. (Since the time averaged power is the same, the degree of dissociation is roughly the same.) The longer afterglow period for the lower PRFs allows T_e to decay to smaller values. For example, the electron temperature was ≈ 0.3 eV and the plasma potential was ≈ 3 V for 20 kHz at the end of the afterglow, while for 5 and 10 kHz, the electron temperature and plasma potential were 0.04 and 0.3 V, respectively.

The electron temperature and plasma potential at the time of the peak in electron temperature are shown in Fig. 8 for different PRFs. The electron temperature and plasma potential peak under the coil at the leading edge of the power-on period, and these localized peaks are more pronounced for lower PRF. Due to a longer period of dissociative attachment during the afterglow at lower PRF, a lower electron density is produced at the end of the afterglow. When the power is turned on, the local power deposition in the high electric fields near the coil occurs in a smaller inventory of electrons, resulting in a higher electron temperature. The localization of electron temperature at low PRF results from a lower thermal conductivity and a shorter energy relaxation length at the higher temperature.

The effect of pressure on plasma properties was investigated from 10 to 30 mTorr, for a peak power of 300 W, PRF of 10 kHz, and duty cycle of 50%. As the pressure is lowered, the electron temperature generally increases during the power-on period due to higher rates of loss by diffusion. The

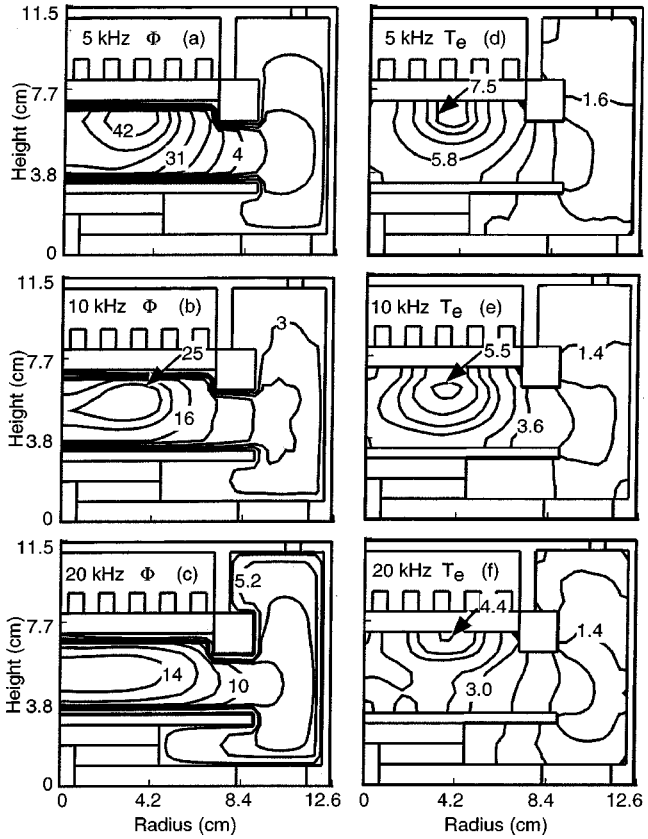

FIG. 8. Plasma potential (a)–(c) and electron temperature (d)–(f) in Ar/Cl_2 plasmas at the time when the peak in electron temperature occurs during the leading edge of the power pulse as a function of PRF for a peak input power of 300 W and duty cycle of 50%.

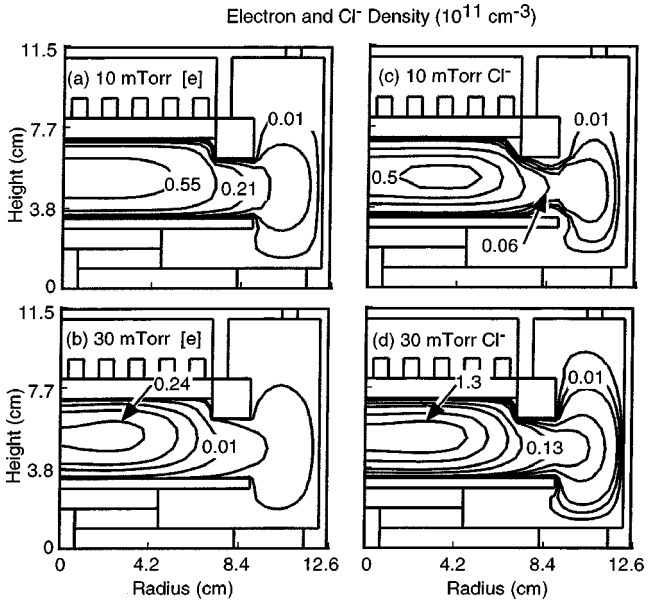

FIG. 9. Electron density (a)–(b) and Cl^- density (c)–(d) in Ar/Cl_2 plasmas in the late afterglow as a function of pressure for a peak power of 300 W, PRF of 10 kHz, and duty cycle of 50%. Results are shown for the end of afterglow for 10 and 30 mTorr. The plasma is more electronegative at higher pressures.

plasma potential scales similarly to the electron temperature. As the electron temperature and plasma potential rise at the leading edge of the power pulse, the high electron temperature is more conducive to device damage. Fortunately, the flux of these electrons to the substrate is low. The peak electron temperature was 5.5 eV and plasma potential was 42 V at 10 mTorr, while at 30 mTorr, these values were 5 eV and 32 V. The electron temperatures in the late afterglow were about 0.5 and 0.042 eV at 10 and 30 mTorr, respectively, a consequence of higher rates of thermalizing collisions at the higher pressure.

The spatiotemporal evolution of electron and Cl^- density varies with pressure tracking the electron temperature. For example, the electron and Cl^- densities in the late afterglow are shown in Fig. 9 for 10 and 30 mTorr. At power turn on, the Cl^- density at the reference point has a more prominent peak at higher pressure as a larger number of negative ions at the end of the afterglow move to the center of the reactor. In the late active glow at higher pressures, the rate of production of electrons is lower and the rate of attachment is higher due to the lower electron temperature, resulting in a lower electron density. The maximum Cl^- density was 1.3×10^{11} cm^{-3} at 30 mTorr at the end of the afterglow, while only 5×10^{10} cm^{-3} at 10 mTorr. The electron density was 2.4×10^{10} cm^{-3} at 30 mTorr and 5.5×10^{10} cm^{-3} at 10 mTorr. The plasma is therefore generally more electronegative in the afterglow at higher pressures and the plasma potential is lower, thereby making it easier to extract negative ions.

The consequences of electronegativity of the feedstock gases were investigated by varying the Cl_2 mole fraction from 20% to 70%. As the Cl_2 fraction increased, the plasma more rapidly transitioned to an ion–ion composition in the afterglow. For example, the ratio of electron density to positive ion density at the end of the afterglow and as a function is time is shown in Fig. 10. As the Cl_2 fraction increased from 20% to 70%, this ratio decreased from 0.25 to 1.7×10^{-5} at the end of the afterglow. An $[e]/[M^+]$ of <0.01, a measure of a true ion–ion plasma, occurs here for a Cl_2 mole fraction >0.35. The transition to an ion–ion plasma occurs more rapidly as the Cl_2 mole fraction is increased due to the higher rate of attachment. For a 20% Cl_2, the transition to an ion–ion plasma requires a longer off period than provided by this PRF and duty cycle.

Note that at power on, the electron density rapidly decreases before recovering for the larger Cl_2 mole fractions which have transitioned to an ion–ion plasma by the end of the afterglow. This rapid decrease in electron density occurs because the electron density is sufficiently low at the end of the afterglow that space charge neutrality is maintained largely by the negative ions. The ambipolar electric fields are only of sufficient magnitude to maintain a balance of negative ion and positive ion fluxes leaving the plasma. As a consequence, electrons are to a large part in a free diffusion mode. When the power is applied there is a short period of time (a few μs) during which the electrons are heated by the high fields and achieve a high electron temperature and correspondingly higher rate of diffusion, but ionization has yet

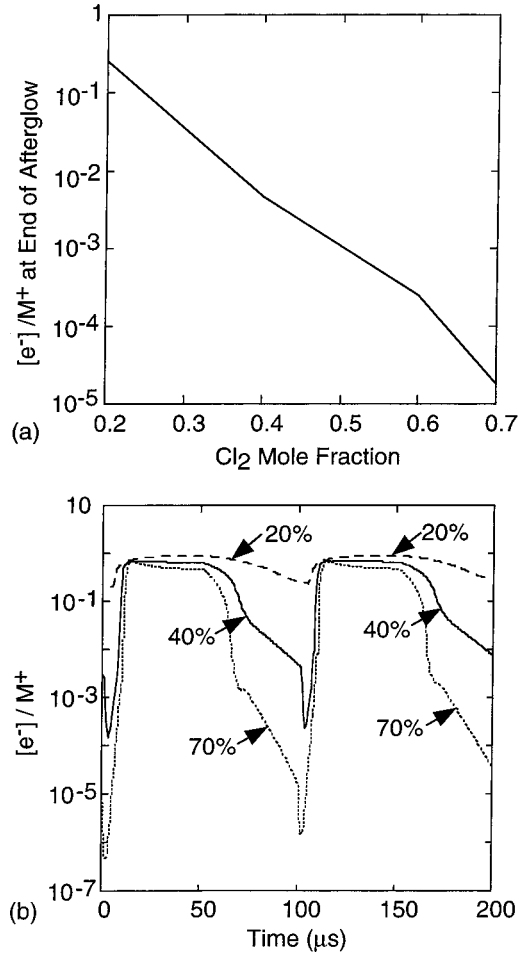

FIG. 10. Ratio of electron density to positive ion density: (a) at the end of the afterglow (just before power turn on) as a function of the Cl_2 mole fraction and (b) as a function of time for different Cl_2 mole fractions. As the Cl_2 mole fraction increases, the plasma transitions to an ion–ion plasma earlier during the afterglow.

to occur in significant amounts. The ambipolar fields are therefore still ''sized'' to balance the ion fluxes. The hotter electrons, unimpeded by the weak ambipolar fields, are lost more rapidly by diffusion. Once sufficient electron avalanche has occurred so that electrons once again are major contributors to the charged particle density, the larger ambipolar electric fields reestablish themselves to confine the electrons.

The fluxes of positive ions, electrons, and Cl^- ions to the substrate are shown as a function of time for different Cl_2 fractions in Fig. 11. In the active glow, the plasma is electropositive, thereby resulting in nearly equal fluxes of electrons and positive ions to the substrate. The flux of negative ions to the substrate is negligible during the active glow as the plasma potential is sufficiently positive to confine negative ions. As the plasma potential drops to below a few volts in the afterglow, the sheath potential becomes sufficiently small that negative ions can be extracted. Negative ion extraction occurs later into the afterglow as the Cl_2 fraction decreases and the transition to the ion–ion plasma takes longer to occur. Significant Cl^- extraction is only obtained for Cl_2 mole fractions >0.5

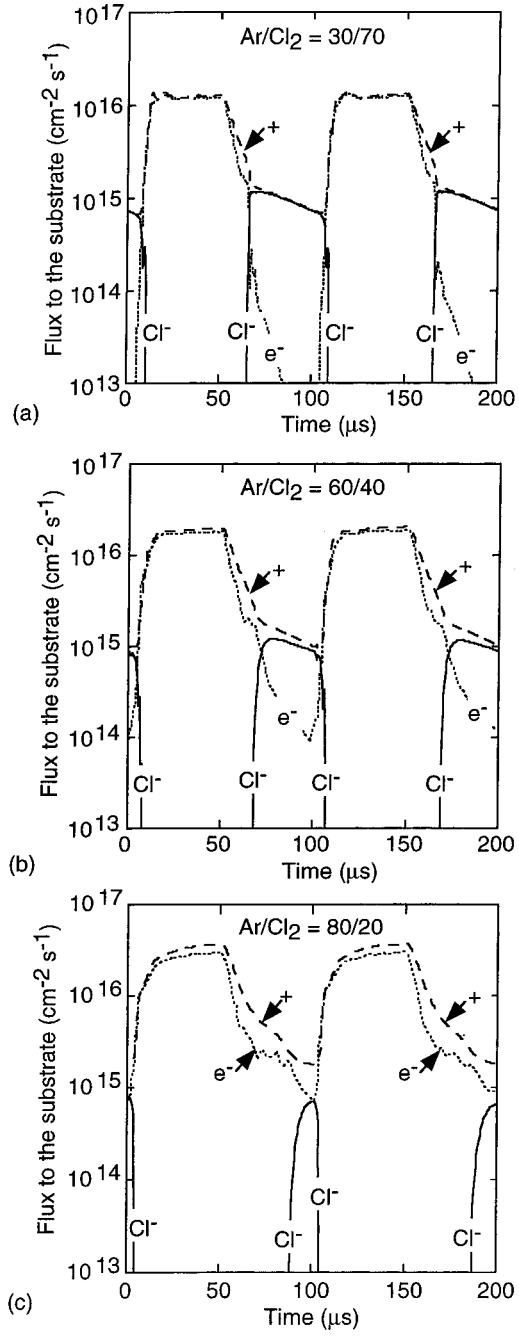

FIG. 11. Temporal dynamics of the positive ion, electron, and Cl^- fluxes to the substrate as a function of Cl_2 mole fraction: (a) $Ar/Cl_2=30/70$, (b) $Ar/Cl_2=60/40$, and (c) $Ar/Cl_2=80/20$. As the Cl_2 more fraction increases, negative ions can be extracted for longer periods during the afterglow.

IV. CONCLUDING REMARKS

Results from a computational investigation of pulsed operation of ICPs in Ar/Cl_2 mixtures were discussed. We found that the peak electron temperature at the leading edge of the power-on pulse increases with a decrease in duty cycle as the same power is deposited into a smaller number of electrons. As the Cl_2 fraction increases this peaking of electron temperature is more pronounced as there are fewer surviving electrons at the end of the afterglow. As the pressure is lowered, the electron temperature and plasma potential at the

leading edge of the power on pulse increase as well. As the PRF decreased, the peak in electron temperature increased as the electron density at power on was proportionally smaller. The spatial distribution of electron temperature showed a larger peak under the coils at lower PRFs as the conductivity of the plasma was lower, particularly at high Cl_2 fraction. The inertia of Cl^- ions made them unable to respond to rapid changes in the plasma potential, which resulted in ''islands'' of higher Cl^- density in the periphery of the reactor. As the Cl_2 fraction increases, the transition from an electron–ion to ion–ion plasma in the afterglow is more rapid and pronounced. As the Cl_2 fraction decreases, there is less attachment and electron flux persists for longer times in the afterglow, which delays the extraction of negative ions. For the conditions investigated (PRF$=10$ kHz, duty cycle 50%) negative ions can only be extracted for Cl_2 fractions of >0.5.

ACKNOWLEDGMENTS

This work is supported by the National Science Foundation (Grant No. CTS99-74962), the Semiconductor Research Corp, DARPA/AFOSR, and Applied Materials.

[1]L. J. Overzet, B. A. Smith, J. Kleber, and S. K. Kanakasabapathy, Jpn. J. Appl. Phys., Part 1 **36**, 2443 (1997).
[2]S. Samukawa and T. Meino, Plasma Sources Sci. Technol. **5**, 132 (1996).
[3]S. Samukawa and H. Ohtake, J. Vac. Sci. Technol. A **14**, 3049 (1996).
[4]S. Samukawa, Appl. Phys. Lett. **68**, 316 (1996).
[5]K. Takahashi, M. Hori, and T. Goto, Jpn. J. Appl. Phys., Part 2 **34**, L1088 (1993).
[6]T. Meino and S. Samukawa, Plasma Sources Sci. Technol. **6**, 398 (1997).
[7]M. V. Malyshev, V. M. Donnelly, J. I. Colonell, and S. Samukawa, J. Appl. Phys. **86**, 4813 (1999).
[8]M. V. Malyshev and V. M. Donnelly, Plasma Sources Sci. Technol. **9**, 353 (2000).
[9]P. Subramonium and M. J. Kushner, J. Vac. Sci. Technol. A **20**, 313 (2002).
[10]P. A. Miller, G. A. Hebner, K. E. Greenberg, and P. D. Pochan, J. Res. Natl. Inst. Stand. Technol. **100**, 427 (1995).
[11]R. L. Kinder and M. J. Kushner, J. Vac. Sci. Technol. A **19**, 76 (2001).
[12]W. Z. Collison and M. J. Kushner, Appl. Phys. Lett. **68**, 903 (1996).
[13]S. Rauf and M. J. Kushner, J. Appl. Phys. **81**, 5966 (1997).
[14]Kuck and Associates, Inc. http://www.kai.com/parallel/kappro/
[15]G. A. Hebner and C. B. Fleddermann, J. Appl. Phys. **82**, 2814 (1997).
[16]K. Tachibana, Phys. Rev. A **34**, 1007 (1986).
[17]D. Rapp and P. Englander-Golden, J. Chem. Phys. **43**, 1464 (1965).
[18]R. H. McFarland and J. D. Kinney, Phys. Rev. **137**, 1058 (1965).
[19]G. L. Rogoff, J. M. Kramer, and R. B. Piejak, IEEE Trans. Plasma Sci. **14**, 103 (1986).
[20]Y. Ikezoe, S. Matsuoka, M. Takabe, and A. Viggiano, *Gas Phase Ion-Molecule Reaction Rate Constants Through 1986* (Mass Spectroscopy Society of Japan, Tokyo, 1987).
[21]NIST Chemical Kinetics Database 17, Version 2Q98, http://kinetics.nist.gov/index.php
[22]H. W. Ellis, R. Y. Pai, E. W. McDaniel, E. A. Mason, and L. A. Viehland, At. Data Nucl. Data Tables **17**, 177 (1976).